Int. J. Multiphase Flow, Vol. 7, pp. 179–190, 1981
Printed in Great Britain

0301-9322/81/020179-12$02.00/0
Pergamon/Elsevier

MOMENTUM AND HEAT TRANSFER IN TWO-PHASE BUBBLE FLOW—II

A COMPARISON BETWEEN EXPERIMENTAL DATA AND THEORETICAL CALCULATIONS

Y. SATO and M. SADATOMI
Department of Mechanical Engineering, Kumamoto University, Kumamoto, Japan 860

and

K. SEKOGUCHI
Department of Chemical Engineering, Kyushu University, Fukuoka, Japan 812

(*Received* 24 *May* 1980; *in revised form* 15 *August* 1980)

Abstract—Momentum and heat transfer process in a two-phase air–water bubble flow is investigated experimentally to confirm the applicability of the theoretical model proposed in Part I of this study. Comparisons are made between the measurements and the predictions for both velocity and temperature profiles, and then satisfactory agreement is obtained. Also, the results for bubble flow simulation are presented to clarify the interrelationship of the frictional pressure gradient and the heat transfer coefficient with the void fraction profile.

1. INTRODUCTION

In any flow regime of two-phase gas–liquid flow the momentum and heat transfer process is closely related to the phase distribution properties. It is thus desirable to construct a set of models capable of solving simultaneously the flow, heat transfer and phase distribution problems involved. However, the complexity of flow makes such approach partly difficult. The situation is quite the same in bubble flow. As yet, few satisfactory models exist which would predict the phase distribution and the velocity and temperature fields synthetically.

The phase distribution characteristics of bubble flow is usually specified by the void fraction profile and the size distribution of the bubbles. It has been found experimentally that these parameters depend greatly on flow conditions, for instance, flow rates of both phases, bubble generation method, flow direction as well as physical properties of the fluids (e.g. Sato & Sadatomi 1977). Then, it appears that the prediction of the void fraction distribution in this flow is very hard at present, to be applicable to various flow conditions encounted in practical systems.

Taking account of these aspects, a theory has been proposed in the previous report of this study (Sato *et al.* 1980), which is able to predict the velocity and temperature fields of a bubble flow on condition that the void fraction profile has been prescribed. The essential point of the theory is such that the eddy diffiusivity to express the turbulent structure of the liquid phase is subdivided into the two components, one for the inherent wall turbulence independent of bubble agitation and the other for the additional turbulence caused by bubbles. Although in the previous paper a few comparisons have been made between the predicted and experimental velocity distributions especially for viscous bubble flows of the low liquid Reynolds number, there is still a need to make further comparisons with available experiments to confirm the proposed model as a whole. The main objective of the present paper is then to test the validity of the theory for both the momentum and heat transfer, examining the fully developed turbulent bubble flow in a circular pipe.

For examination of the hydrodynamic portion of the theory, an experiment was performed for a 26-mm i.d. vertical pipe. Comparisons are made between measurements and theoretical predictions of the velocity distribution and the frictional pressure gradient. The existing data of other investigators are also referred as far as possible.

The heat transfer part of the theory is examined by comparing the predicted temperature distributions and the heat transfer coefficients with the experimental data reported by Hinata (1979) and Sekoguchi *et al.* (1980).

2. EXPERIMENT

2.1 *Apparatus*

Experiments were carried out for vertical upward bubble flows in a circular pipe using air and distilled water as the working fluids. A sketch of the essential part of the test rig is shown in figure 1. The test section was made of acrylic resin pipes with a smooth surface wall and an i.d. of $D = 26$ mm.

After leaving an orifice flow meter, water flowed into the pipe at the bottom end, then passed through an entrance section of 1.2 m and reached a two-phase mixer. Following a rotameter, air was introduced continuously into a water stream through the mixer, in which there were 60 holes of each 0.3 mm dia. drilled on the periphery of the pipe (distributed by 4-holes/cm^2). Two-phase bubbly mixture flowed upward in the test section, then passed through a flow measuring section located at a downstream distance of 4.3 m from the mixer, and finally discharged into a separator. Separated air then issued into the atmosphere, while the drainage was led to a weighing tank to check the flow rate.

There were three cocks in the test section arranged in series for hold-up measurement, all of which were linked by a lever to operate simultaneously. The most upstream one served for the two-phase mixture to bypass the test section.

A flow pattern view box was constructed, enclosing a 0.3 m section near the measuring section. The rectangular box, filled with distilled water, removed much of the distortion created by the curvature of pipe. It permitted the determination of bubble size.

2.2 *Measurements*

Air volume fraction $\hat{\alpha}$ was determined by hold-up method; the volume of water, trapped by the two isolation cocks arranged at a distance 1.5 m apart, was measured. The reproducibility of the measurement was within 2 per cent for a case of bubble flow.

Pressure gradient was obtained from the static pressure difference ΔP between two taps, placed before and behind the measuring section at an interval of $\Delta x = 1.16$ m. This pressure differential was detected with a water manometer, using a telescopic micrometer. A capillary vinyl tube of 1.4 mm i.d. in reasonable length lay within the pressure leads, so that the viscous damping of water in this tube eliminated undesirable fluctuations of the meniscus in the manometer and thus it made the pressure differential measurement easy. Frictional pressure gradient and also wall shear stress were determined from the static pressure gradient by means

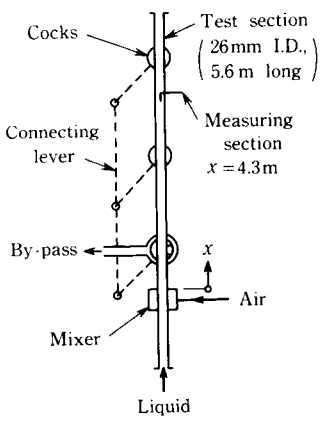

Figure 1. Schematic diagram of test section.

of the following equations, assuming that the static pressure is constant in a cross section and the accelerational pressure gradient and the weight of air are neglibible:

$$\left(\frac{\Delta P_f}{\Delta x}\right) = \left(\frac{\Delta P}{\Delta x}\right) - \rho_L g(1-\hat{\alpha}) \quad [1]$$

$$\tau_w = \frac{D}{4}\left(\frac{\Delta P_f}{\Delta x}\right). \quad [2]$$

Void fraction distribution was measured at the measuring section by use of an electrical resistivity probe which had a phase detecting electrode tip of 0.26 mm dia. The output signals were analyzed with an electronic digital counter. Then, each local void fraction detected by the above system was corrected empirically as described below. Multiplying the originally detected value α_0 by the correction factor C_α, a true local void fraction α is written as

$$\alpha = C_\alpha \alpha_0. \quad [3]$$

Furthermore, if C_α is assumed to be constant over the cross section, it can be obtained from the following equation for a fully developed flow:

$$C_\alpha = R^2\hat{\alpha}/2\int_0^R \alpha_0 r\,\mathrm{d}r, \quad [4]$$

where r is the radial distance and R the pipe radius. The assumption of a constant C_α may be reasonable as far as a drastic change in the phase properties does not take place in the cross section. Accordingly, the void fraction profile was determined from [3] and [4] with the aid of the measured air volume fraction $\hat{\alpha}$. In the practice, the value of this correction factor ranged from 0.90 to 1.01.

Liquid velocity was measured by means of an impact pressure probe. The probe, which was an L-shaped capillary tube of 0.55 mm i.d. and 0.80 mm o.d., was attached to its own traversing mechanism and directed toward upstream to detect the total pressure. The impact pressure was obtained by reading the differential between the total pressure and the static pressure at the wall. Then, the liquid velocity was determined by use of the following equation suggested by Shires & Riley (1966):

$$u_{L0} = \sqrt{\left(\frac{2}{(1-\alpha^2)}\frac{\Delta P}{\rho_L}\right)} \quad [5]$$

in which ΔP is the impact pressure, α the local void fraction and ρ_L the liquid density.

The correction for u_{L0} was made in a similar manner as to the void fraction. Another correction factor C_u was defined so that a true local liquid velocity u_L was obtained from

$$u_L = C_u u_{L0}. \quad [6]$$

The liquid flow rate evaluated from integration of the velocity distribution should be equal to that of the prescribed value when the flow is steady. Thus, if C_u is assumed to be constant at any position, it can be determined by

$$C_u = Q_L/2\pi\int_0^R (1-\alpha)u_{L0} r\,\mathrm{d}r \quad [7]$$

where Q_L is the liquid flow rate. The range of this value was from 0.94 to 1.05 in the present experiment.

In addition to the above-mentioned impact pressure probe, a hot-film anemometer was utilized. It was considered, however, that the results obtained by this method should only be by way of supplementary information since it was impossible to retain the satisfactory accuracy particularly at high bubble frequencies. The anemometer functioned so as to keep the temperature of a hot-film element to be constant. The probe was a conical shaped sensor (#1231W of Thermo System Co.). In operation, it was discernible whether the probe tip contacted with the water or the air; the output falls off whenever the tip pierces each air bubble. Thus, the output signals were performed averaging except for those corresponding to bubbles, and the result was taken to be the raw data of the local liquid velocity u_{L0}. Finally, its correction was made based on [6] and [7].

Outlet water temperature was read from a mercury-in-glass thermometer placed in the separator. This temperature was used to evaluate physical properties of the fluids.

3. LIQUID VELOCITY DISTRIBUTION

3.1 *Comparison between experiments and predictions*

Figures 2 and 3 show comparisons of the liquid velocity distributions predicted by the theory with those obtained experimentally: figures 2(a)–(c) are concerned with the present experiment, whereas figures 3(a)–(c) are related to the experimental results of other in-

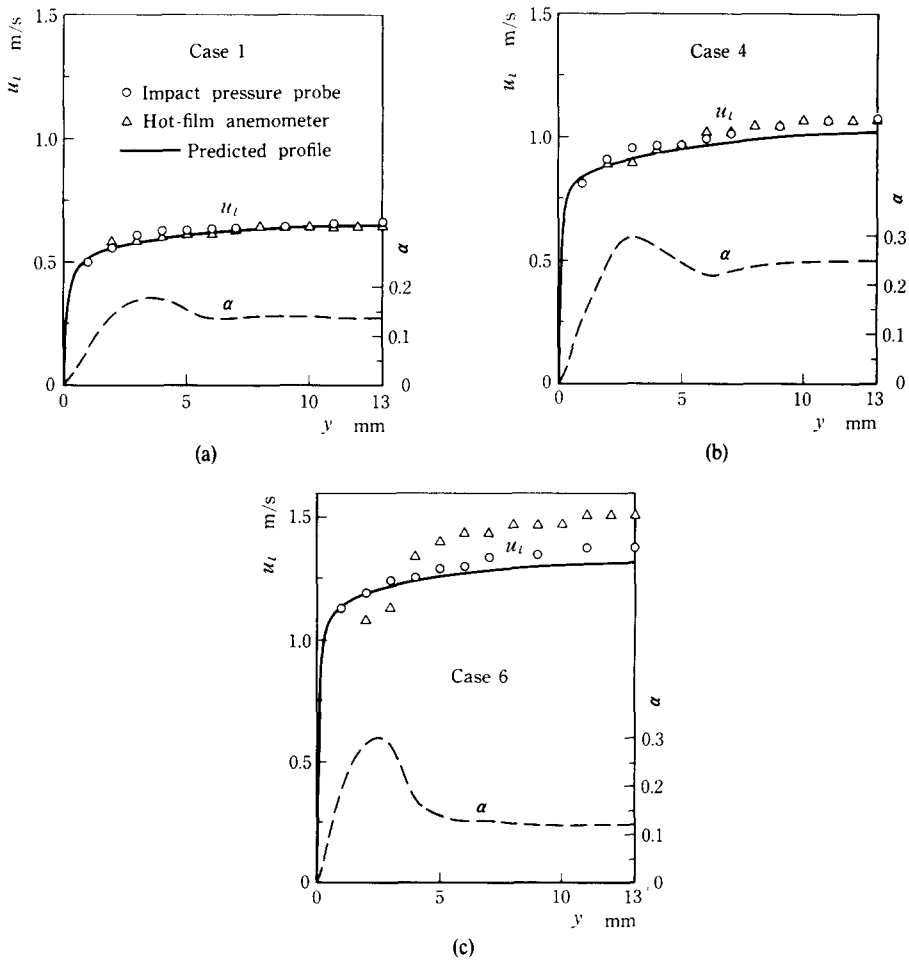

Figure 2. Comparison of the predicted liquid velocity distribution with the present data; ○, with an impact pressure probe; △, with a hot-film anemometer. Corresponding flow parameters are listed in table 1.

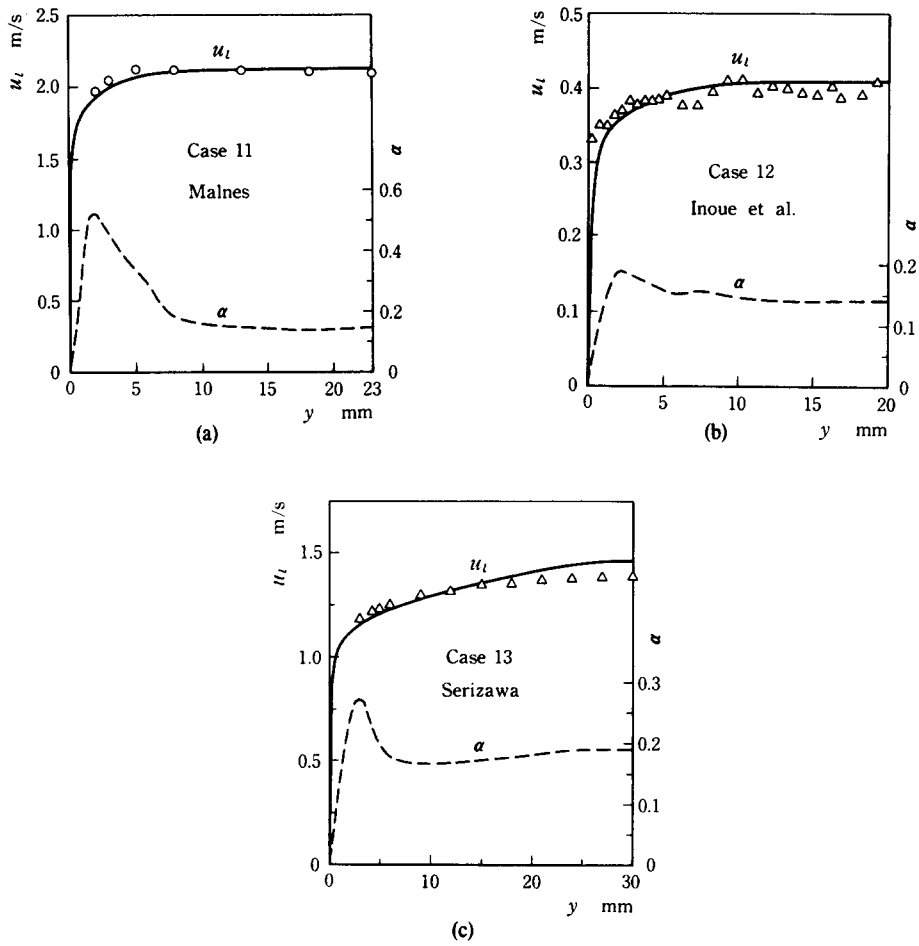

Figure 3. Comparison of the predicted liquid velocity distribution with the data of Malnes (1966), Inoue *et al.* (1976) and Serizawa *et al.* (1975); O, with an impact pressure probe; Δ, with a hot-film anemometer. Corresponding flow parameters are listed in table 1.

vestigators (Malnes 1966), Serizawa *et al.* 1975 and Inoue *et al.* 1976). Principal flow parameters corresponding to each case are listed in table 1, which includes also the data for a few other flows omitted in the figures. (Cases 1–6 belong to the present experiment, while Case 11–15 to the others.) In every figure the data points are labeled according to the instrumentation; open circles are with an impact pressure probe and triangles are with a hot-film anemometer. Each solid curve represents the predicted liquid velocity distribution and also dashed curve does the void fraction profile determined experimentally. The equations used for this calculation are as follows (Sato *et al.* 1980);

$$\frac{du_L^+}{dy^*} = \frac{\tau^*}{(1-\alpha)(\nu_L + \epsilon' + \epsilon'')/Ru_L^*} \qquad [8]$$

$$\tau^* = \left(1 - B\int_0^1 \alpha r^* \, dr^*\right) r^* + \frac{B}{r^*}\int_0^{r^*} \alpha r^* \, dr^* \qquad [9]$$

$$\epsilon' = 0.4\left\{1 - \exp\left(-\frac{y^+}{A^+}\right)\right\}^2 \left\{1 - \frac{11}{6}\left(\frac{y^+}{R^+}\right) + \frac{4}{3}\left(\frac{y^+}{R^+}\right)^2 - \frac{1}{3}\left(\frac{y^+}{R^+}\right)^3\right\} \nu_L y^+ \qquad [10]$$

$$\epsilon'' = 1.2\left\{1 - \exp\left(-\frac{y^+}{A^+}\right)\right\}^2 \alpha \left(\frac{d_B}{2}\right) U_B . \qquad [11]$$

Table 1. Flow parameters for the experiments shown in figures 2 and 3

Case	j_ℓ [m/s]	j_g [m/s]	$T_{\ell b}$ [°C]	Press. [MPa]	$\hat{\alpha}$ [-]	τ_w [Pa] Exp.	τ_w [Pa] Cal.	$\hat{d}_B$ [mm]	D [mm]	Remarks
1	0.50	0.056		0.115	0.071	1.65	1.24	4.4		
2	0.50	0.105		0.115	0.131	2.14	1.47	4.8		
3	0.70	0.104	30.0	0.115	0.102	3.09	2.51	4.5	26.0	Present data *)
4	0.70	0.244		0.114	0.222	4.43	3.74	5.6		
5	1.00	0.104		0.116	0.083	4.95	5.11	4.0		
6	1.00	0.243		0.115	0.173	6.46	6.46	4.6		
11	1.50	0.643	16.5	0.155	0.260	9.52	14.28	3.0	46.0	Malnes (1966) **)
12	0.32	0.085	(20.0)	(0.147)	0.150	10.87	0.74	(3.5)	40.0	Inoue et al. (1976) ***)
13	1.03	0.277	(20.0)	(0.103)	0.178	-	4.91	(4.0)	60.0	Serizawa et al. (1975) ***)
14	1.00	0.101	17.9	0.130	0.069	3.64	3.32	3.4	35.4	Sekoguchi et al. (1975) **)
15	1.00	0.207	22.0	0.120	0.117	5.69	5.86	3.5	34.8	Sato et al. (1975) **)

( ) : Estimated values.
*) : Liquid velocity measurement ; Impact pressure probe method and hot-film anemometer
**) : Liquid velocity measurement ; Impact pressure probe method.
***) : Liquid velocity measurement ; Hot-film anemometer.

τ^* is the dimensionless shear stress distribution, the ratio of the local value to the wall shear stress. ϵ' and ϵ'' are the eddy diffusivities to express the inherent wall turbulence independent of bubble agitation and the additional turbulence caused by bubbles, respectively. Also, α is the local void fraction, d_B the bubble dimension (see [22] in Part I), U_B the terminal velocity of bubble in the quiescent liquid, u_L^* the friction velocity, and $B = gR/u_L^{*2}$. u_L^+, y^+, y^* and r^* are defined as

$$u_L^+ = u_L/u_L^* \qquad [12]$$

$$y^+ = = u_L^* y/\nu_L \qquad [13]$$

$$y^* = y/R \qquad [14]$$

$$r^* = 1 - y/R. \qquad [15]$$

The method for the numerical calculation has been presented in detail in the previous paper.

Each predicted curve is seen to be in good agreement with the experimental result except for figure 2(c), Case 6. In this case there is a disparity between the data points, the open circles with an impact pressure probe and the triangles with a hot-film anemometer. As mentioned in section 2.2, the latter measurement may be inadequate because of the high bubble frequency, at which the output signals became indiscernible indicating whether the liquid or gas phase.

In addition, it is found from the table that the calculated value for each wall shear stress τ_w is in reasonable agreement with the measurement, with a few exception perhaps to be subject to error in measurement.

From the above comparison, it can be concluded that [8] together with [9]–[11] is applicable with success to the description of bubble flow. Moreover, it may be reasonable to expect that the flow in the region close to the wall can be described by these equations, though any experimental information about the velocity has not been available yet.

3.2 *Cross-sectional distribution of flow parameters*

As a typical example, figures 4(a) and 4(b) show the predicted distributions of the shear stress τ^*, the dimensionless coefficient of diffusivities ϵ_{TP}^* and ϵ_l^* as well as the liquid velocity

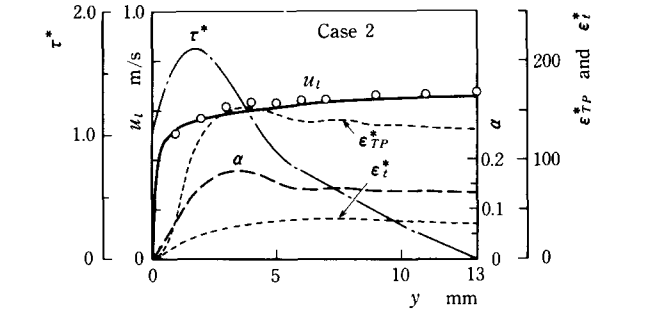

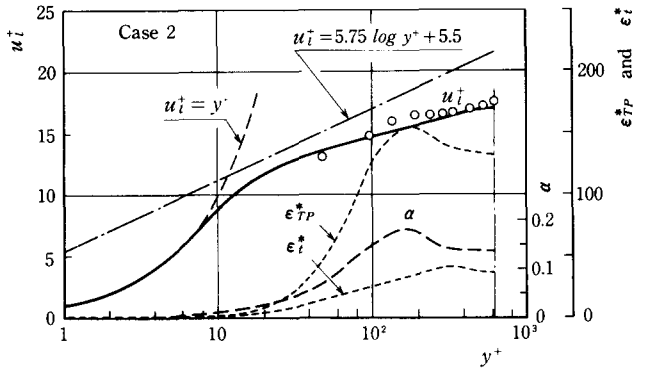

Figure 4. Distribution of flow parameters in a typical bubble flow: results for the liquid velocity u_L, shear stress τ^*, and eddy diffusivities ϵ^*_{TP} and ϵ^*_l of Case 2. The measured liquid velocity and void fraction are also plotted.

u_L for Case 2. ϵ^*_{TP} and ϵ^*_l are defined as

$$\epsilon^*_{TP} = (1-\alpha)(\nu_L + \epsilon' + \epsilon'')/\nu_L \qquad [16]$$

$$\epsilon^*_l = (1-\alpha)(\nu_L + \epsilon')/\nu_L . \qquad [17]$$

The experimental values for void fraction α and liquid velocity u_L are presented by the dashed curve and the open circles, respectively. The abscissa of figure 4(a) is distance from the wall y marked with equal division, while that of figure 4(b) is the dimensionless distance y^+ graduated by logarithm in order to show the trends in the wall region more clearly.

As seen from the figures, the total coefficient of diffusivity ϵ^*_{TP} depends on the local void fraction. And, in this flow the difference between ϵ^*_{TP} and ϵ^*_l is significant, which presents the contribution of bubble agitation. It appears that such effect of bubble agitation becomes dominant at a low liquid flow rate, because decreasing values of the liquid Reynolds number, $\mathrm{Re}_L = j_L D/(1-\hat{\alpha})\nu_L$, correspond to decreasing values of ϵ' and, on the other hand, Re_L has little effect on ϵ''. (j_L is the volumetric flux density of the volumetric flux density of the liquid phase.)

The shape of void fraction profile influences the shear stress distribution. In a case where a void fraction profile has a peak near the pipe wall such as this example, the local shear stress does not decrease monotonously in its value toward the pipe center, but has a peak adjacent to the wall as seen in figure 4(a). Then such local shear stress τ^*, together with ϵ^*_{TP}, determines the liquid velocity gradient.

The well-known logarithmic velocity distribution,

$$u_L^+ = 5.75 \log y^+ + 5.5 , \qquad [18]$$

is drawn on figure 4(b) to be compared with that of the bubble flow. There is an evident discrepancy between these two velocity distributions.

4. LIQUID TEMPERATURE DISTRIBUTION

Figures 5 and 6 show comparisons of the liquid temperature distribution predicted by the theory with the experimental data of Hinata (1979) and Sekoguchi *et al.* (1980), both of which are concerned with vertically upward bubbly flows heated under a constant heat flux condition. The corresponding flow parameters in each case are listed in table 2. In each figure, open circles are the data points of liquid temperature; the solid line and the dot–dash line represent the calculated profiles of the temperature and velocity of the liquid phase respectively; the dashed curve shows the measured void fraction profile. The basic equation for the liquid temperature has been obtained in the dimensionless form (Sato *et al.* 1980):

$$\frac{dT_L^*}{dy^*} = -\frac{1}{2}\mathrm{Nu}\frac{q^*}{(1-\alpha)\left\{1+\mathrm{Pr}_L\left(\frac{\epsilon'+\epsilon''}{\nu_L}\right)\right\}} \qquad [19]$$

in which T_L^* is the dimensionless local liquid temperature, q^* the ratio of the local to the wall heat flux, Nu the Nusselt number, and ϵ' and ϵ'' the eddy diffusivities for heat which are taken to be equal to those momentum in this study, given by [10] and [11] respectively. T_L^*, Nu and

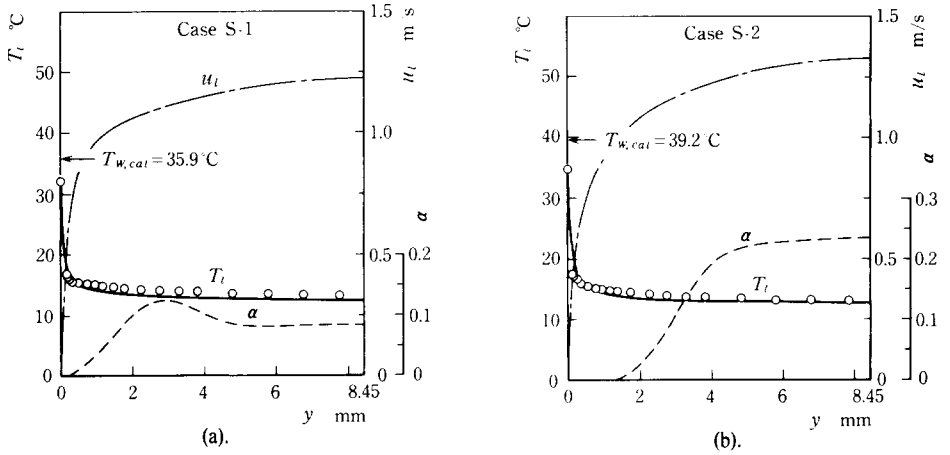

Figure 5. Comparison of the predicted liquid temperature distribution with the experimental data of Sekoguchi *et al.* (1980). The measured void fraction α and the predicted liquid velocity distribution u_L are also given. (Corresponding flow parameters are listed in table 2.)

Table 2. Principal parameters for the experiments with heat addition shown in figures 5 and 6

Case	j_ℓ [m/s]	j_g [m/s]	$\hat{\alpha}$ [-]	$\hat{d}_B$ [mm]	q_{w_2} [kW/m^2]	$T_{w,Exp.}$ [°C]	$T_{\ell b}$ [°C]	h_{TP} [kW/m^{2}K] Exp.	Cal.	D [mm]	Remarks
S-1	0.93	0.13	0.078	2.4	117	32.4	13.6	6.24	5.25		Fig. 5(a)
S-2	0.93	0.13	0.097	4.0	118	34.6	13.6	5.64	4.63	16.9	Fig. 5(b)
S-3	0.93	0.33	0.19	2.8	119	29.2	13.7	7.64	5.65		
S-4	0.93	0.32	0.19	4.2	120	31.4	13.8	6.81	5.22		
H-1	0.50	0.18	0.24	4.3	37.1	41.5	34.8	5.58	6.35		
H-2	0.84	0.043	0.046	4.2	33.6	42.2	34.9	4.58	6.69		Fig. 6(a)
H-3	0.84	0.13	0.13	3.6	33.6	41.2	35.0	5.43	7.33	38.5	
H-4	0.84	0.17	0.18	3.6	33.6	40.9	35.0	5.67	9.12		Fig. 6(b)
H-5	2.0	0.17	0.11	3.6	34.6	38.7	34.6	8.47	13.4		

S-1~4 : Sekoguchi et al.(1980), H-1~5 : Hinata(1979).

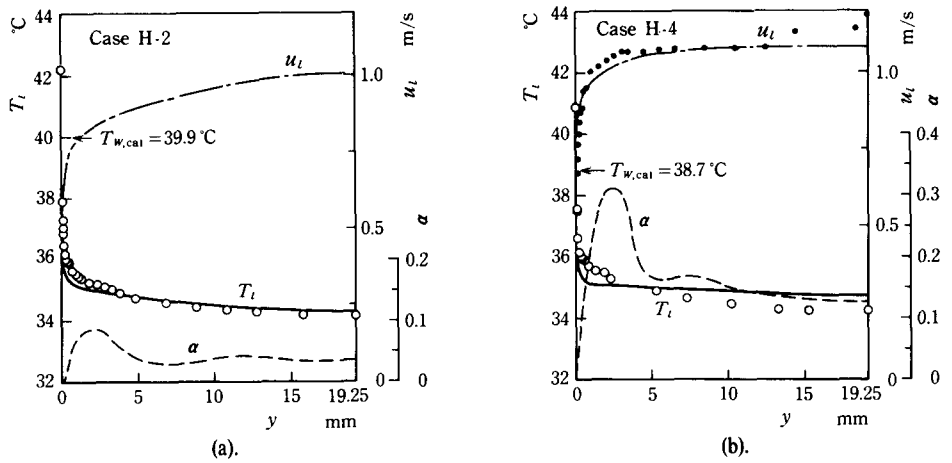

Figure 6. Comparison of the predicted liquid temperature distribution with the experimental data of Hinata (1979). The measured void fraction α and the predicted liquid velocity distribution u_L are also given. In figure 6(b) the measured liquid velocity are also plotted by solid circles. (Corresponding flow parameters are listed in table 2.)

h_{TP} are defined as

$$T_L^* = (T_L - T_{Lb})/(T_w - T_{Lb}) \quad [20]$$

$$\mathrm{Nu} = h_{TP}D/\lambda_L \quad [21]$$

$$h_{TP} = q_w/(T_w - T_{Lb}) \quad [22]$$

where T_{Lb} is the bulk liquid temperature, T_w the wall temperature, h_{TP} the heat transfer coefficient, Pr_L and λ_L the Prandtl number and the coefficient of heat conduction of the liquid. In addition, the physical properties were evaluated at the mean temperature of the bulk and the wall.

As for the available experiments on the whole, it can be said that the prediction gives fairly good results for the liquid temperature distribution. However, there are a few cases in which a noticeable disparity has been observed between the predicted and measured values such as figure 6(b), the measured temperature gradient being appreciably greater than the predicted in the core region. Generally speaking, an agreement on the temperature distribution is not quite so good as that on the velocity. The explanation for this discrepancy probably lies in not only the theoretical model but the measurement. It is believed that, owing to the technical difficulties, the temperature distribution in a diabatic flow was not measured with as much precision as velocity distribution in an adiabatic flow. The major error involved in the experiments may be that of determining the time-averaged liquid phase temperature being free from undesirable signals in contact with the gas bubbles.

The resulted values for both the calculated and measured heat transfer coefficient have been entered in table 2. There exist considerable differences between the data of Hinata (1979) and those of Sekoguchi *et al.* (1980) comparing with each calculated value, the calculated value being higher than the measured in the cases of Hinata's experiment and vice versa in the cases of Sekoguchi's. Therefore, in order to obtain decisive proof of the theoretical model or to discuss it in more detail, further systematic experiments are needed especially for the temperature field with heat addition.

5. DISCUSSION—DEPENDENCE OF BOTH FLOW AND HEAT TRANSFER ON VOID FRACTION PROFILE

In this section the results for simulation of several bubble flows are represented on the basis of the proposed theory. As illustrated in figure 7(a), the six different void fraction profiles labeled as 1–6 have been considered under the same condition described below. The curves 2–6 are the profiles posturated tentatively for the simulation, while the curve 1 alone is a real one determined by an experiment from which a few flow parameters necessary for the calculation were obtained; i.e. $D = 26$ mm, $j_L = 1.0$ m/s, $\hat{\alpha} = 0.12$, $d_B = 4.3$ mm, $T_{Lb} = 24.3$°C. In addition, the heat flux is taken as $q_w = 0.116$ MW/m^2 for the present.

The calculated liquid velocity and temperature distributions corresponding to each void fraction profile are presented in figures 7(b) and 7(c) respectively. (A couple of curves are omitted to avoid confusion.) It is found that, except for the immediate neighborhood of the wall, relatively flat velocity and temperature distribution curves result from a concave void fraction profile such as the curve 1, 2 or 3.

The results for the wall sheat stress τ_w, the wall temperature T_w and Nusselt number Nu of each flow are summerized in table 3. The flow labeled as "0" in this table represents a single-phase water flow with the bulk velocity of $\hat{u}_L = j_L/(1-\hat{\alpha}) = 1.14$ m/s, which facilitates the comparison with the other bubble flows. The wall shear stress and Nusselt number of this flow, τ_{w0} and Nu_0, can also be evaluated by the theory taking any void fraction to be zero. Inspection of table 3 and figure 7 indicates that, if the void fraction profiles are dissimilar, the different

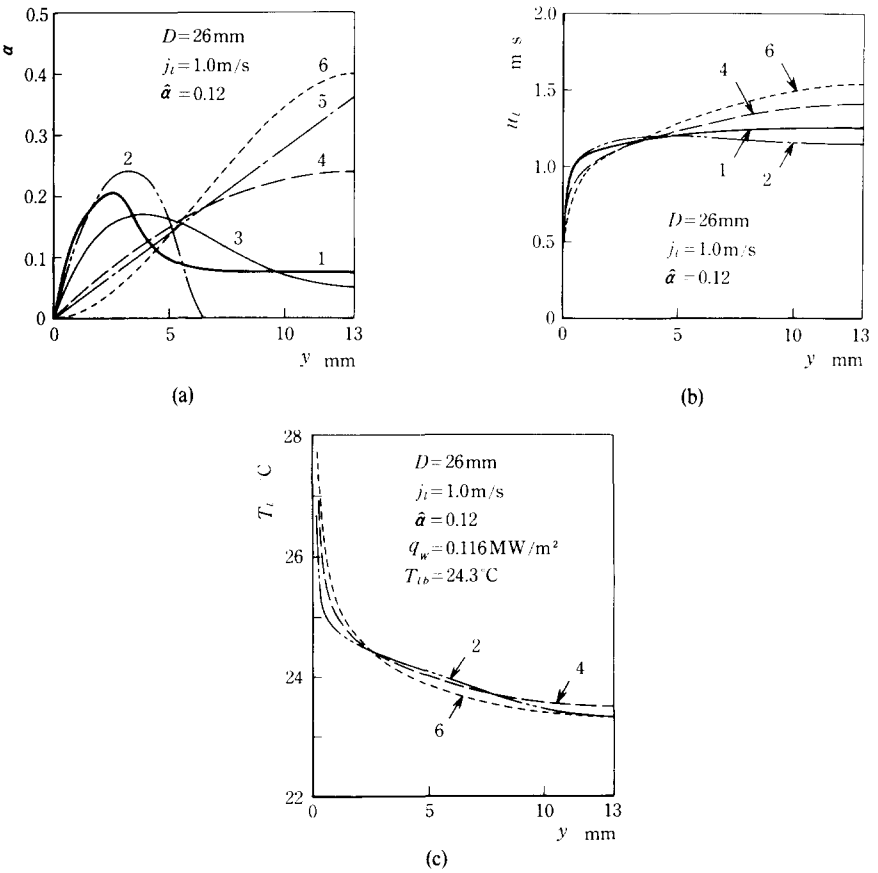

Figure 7. An example as to dependence of the liquid velocity and temperature distribution on the void fraction profile. (a) Given void fraction profiles; the curve 1 is experimentally obtained one, while the others are tentatively posturated ones. (b) Corresponding liquid velocity distributions calculated. (c) Corresponding liquid temperature distributions calculated. (A couple of curves are omitted in both figures 7(b) and 7(c) to prevent confusion.)

Table 3. Dependence of the wall friction and heat transfer on void fraction profile: an example of the calculated results for the wall shear stress, the wall temperature and the Nusselt number corresponding to the void fraction profiles shown in figure 7(a)*)

No. of α-profile in figure 7(a)		0**	1	2	3	4	5	6
τ_w	[Pa]	3.79†	5.66	6.06	5.25	4.14	3.83	3.83
τ_w/τ_{w0}	[-]	1	1.49	1.61	1.38	1.09	1.01	1.01
T_w	[°C]	43.4†	36.6	36.7	37.9	40.4	41.2	43.8
Nu	[-]	262†	405	402	367	309	295	257
Nu/Nu_0	[-]	1	1.55	1.53	1.40	1.18	1.13	0.98

*) Calculating conditions : D=26 mm, j_ℓ=1.0 m/s, $\hat{\alpha}$=0.12, q_w=0.116 MW/m^2, $T_{\ell b}$=24.3 °C and $\hat{d}_B$=4.3 mm.

**) Single-phase water flow of $\hat{u}_\ell=j_\ell/(1-\hat{\alpha})$=1.14 m/s.

†) Estimated value from the proposed theory taking α=0.

values of τ_w and Nu result even under the same flow condition. From the systematic order of these estimated values, it appears that relatively high void fraction near the wall causes higher values of both τ_w and Nu. This trend is consistent with the experimental knowledge on the relationship between void fraction profile and heat transfer in a bubble flow reported by Sekoguchi *et al.* (1980).

5. CONCLUSIONS

A theoretical model for bubble flow, proposed in the previous report of this study (Part I), has been examined by experiments. In addition to the existing data of several other investigators, satisfactorily accurate data on the liquid velocity distribution and the frictional pressure gradient were obtained from the present experiment, performed for 26 mm i.d. vertical pipe with air and water. As the result of comparison, good agreement has been obtained between the data and the predicted values. Thus, it can be concluded that the hydrodynamic portion of the theory has been confirmed to be valid.

The other part of the theory describing heat transfer process has also been tested by comparing the predicted temperature and the heat transfer coefficient against the experimental values reported by Hinata (1979) and Sekoguchi *et al.* (1980). The predicted results are seen to be acceptable, though the detailed agreement between the data and the calculations is not particularly excellent. It should be emphasized here that more systematic and reliable experiments on the temperature field is required to obtain decisive proof of this part of the theory or to improve it.

Acknowledgements—The authors wish to thank Mr. K. Horita for his assistance with the experimental work. This work was partially supported by the research fund (Grant-in-Aid for Cooperative Research 335010) of the Ministry of Education, Science and Culture of Japan.

REFERENCES

HINATA, S. 1979 The measurement of temperature distribution in vertical two-phase air–water flow. (In Japanese) Preprint, *16th Symp. Heat Transfer Society of Japan*, 85–87.

INOUE, A., AOKI, S., KOGA, T. & YAEGASHI, H. 1976 Void-fraction, bubble and liquid velocity profiles of two-phase bubble flow in a vertical pipe. (In Japanese), *Trans. JSME* **42**-360, 2521–2531.

MALNES, D. 1966 *Slip Ratios and Friction Factors in Bubble Flow Regime in Vertical Tubes*, KR-110. Kjeller, Norway.

SATO, Y. & SEKOGUCHI, K. 1975 Liquid velocity distribution in two-phase bubble flow. *Int. J. Multiphase Flow* **2**, 79–95.

SATO, Y., SADATOMI, M. & SEKOGUCHI, K. 1980 Momentum and heat transfer in two-phase bubble flow—I. Theory. *Int. J. Multiphase Flow* **7**, 167–177.

SATO, Y. & SADATOMI, M. 1977 On the variety of the void fraction distribution in two-phase bubble flow. (In Japanese), Preprint, *14th Symp, Heat Transfer Society of Japan*, 316–318.

SEKOGUCHI, K., FUKUI, H., TSUTSUI, M. & MIURA, H. 1975 Investigation into statistical characteristics of bubbles in two-phase flow—4th Report. Experimental results for velocity and void fraction distributions. (In Japanese), *Preprint of JSME* 758-2, 90–93.

SEKOGUCHI, K., NAKAZATOMI, M., SATO, Y. & TANAKA, O. 1980 Forced convective heat transfer in vertical air–water bubble flow. *Bull. JSME* **23**(184), 1625–1631.

SERIZAWA, A., KATAOKA, I. & MICHIYOSHI, I. 1975 Turbulence structure of air-water bubbly flow II. Local properties. *Int. J. Multiphase Flow* **2**, 235–246.

SHIRES, G. L. & RILEY, R. J. 1966 The measurement of radial voidage distribution in two-phase flow by isokinetic sampling. AEEW-M650.